Entropy Analysis and Thermal Characteristics of Reiner Philippoff Hybrid Nanofluidic Flow Via a Parabolic Trough of Solar Aircraft Wings: Keller Box Method

Tanveer Sajid
Capital University of Science and Technology (CUST)
Wasim Jamshed
Capital University of Science and Technology (CUST)
Faisal Shahzad
Capital University of Science and Technology (CUST)
Mohamed R. Eid
New Valley University
Esra Karataş Akgül (esrakaratas@siirt.edu.tr)
Siirt University
Kottakkaran Sooppy Nisar
Prince Sattam bin Abdulaziz University

Research Article

Keywords: Solar Aircraft, PTSC, Thermal radiation, Heat generation

Posted Date: August 4th, 2021

DOI: https://doi.org/10.21203/rs.3.rs-763495/v1

Entropy Analysis and Thermal Characteristics of Reiner Philippoff Hybrid Nanofluidic Flow Via a Parabolic Trough of Solar Aircraft Wings: Keller Box Method

Tanveer Sajid [a], Wasim Jamshed [a], Faisal Shahzad [a], Mohamed R. Eid [b,c], Esra Karataş Akgül [d,*] and Kottakkaran Sooppy Nisar[e]

[a] Department of Mathematics, Capital University of Science and Technology (CUST), Islamabad, 44000, Pakistan.

[b] Department of Mathematics, Faculty of Science, New Valley University, Al-Kharga, Al-Wadi Al-Gadid, 72511 Egypt.

[c] Department of Mathematics, Faculty of Science, Northern Border University, Arar, 1321, Saudi Arabia.

[d] Art and Science Faculty, Department of Mathematics, Siirt University, TR-56100, Siirt, Turkey.

[e] Department of Mathematics, Prince Sattam bin Abdulaziz University, Wadi Aldawaser, 11991, Saudi Arabia.

*Corresponding Author, E. K. Akgül *(esrakaratas@siirt.edu.tr)*

Abstract

Solar energy is about the study of solar radiations and a method to enhance the efficacy of solar aircrafts with the utilization of solar radiations and nanotechnology. Solar radiations has been considered a heat source. The heat transmission performance of the wings is scrutinized for the situation of various effects like thermal radiations, heat generation, variant thermal conductance, thermal conductivity, and viscidness dissipative flow. Entropy generation analysis has been carried out in the status of Reiner Philippoff nanofluid (RPNF). The performance of the solar aircraft wings (SACW) improves in relations of thermal transmission for the status of amplification in thermal radiation, heat generation, viscidness dissipative flowing, and thermal conductivity parameters.

Keywords: *Solar Aircraft, PTSC, Thermal radiation, Heat generation.*

1. Introduction

In agricultural ecosystems, ground solar energy improvements are growing due to the situation of utility-scale improvements of solar energy in previous agricultural areas. A sun always divides water, allows it to evaporate sun heat, cool it off, and then collect water. They are used in areas where there is no drinking water. The clean water is then obtained by showing it in sunlight from polluted water or plants. Many solar organisms also produce big condensed sunscreens and condensation traps. Unclean water is still present in a solar system outside the collector and is

vaporized by transparent plastic or crystal clear sunlight. Solar energy is assisted by the most advantageous green technologies. These systems, however, are heavily climate-dependent creating time gaps between the availability of resources and energy use. In certain implementations such as desalination of salt-water, waste sterilization, and electricity generation, solar energy can be used to constitute steam [1, 2]. Nanotechnology has helped to achieve valuable improvement in these systems' efficiency [3]. The use of appropriate nanofluids would provide useful improvements to the precise operation of these devices. Applying the gold particles to plasmonic nanofluids will increase the precision of the systems by around 300. In solar steam generation systems, Nanofluids with CNTs are the appropriate choices. In a solar direct vapor environment, Wang et al. [4] have applied the SWCNT nanofluid and investigated the impacts of solar energy density and nanofluid levels. They also accomplished that the rate of evaporation has improved by increasing the amount of nanofluid and solar power.

Solar aircraft have a continuous cruise ability of 24 hours and are more visible, less flying speed, and less structural than conventional aircraft. Improvements in aerodynamic characteristics and appropriate structural weight reductions are the main factors in continuous solar aircraft cruising. Solar aircraft have special construction methods, conventional aircraft configuration features and the wings used in solar aircraft are extremely different [5]. Solar energy has a widespread appeal as an environmentally friendly, affordable, and inexhaustible alternative. Parabolic solar technology is the furthermost developed and cost-efficient, highly effective solar energy technology in existence today among three fundamental solar thermal generating systems comprising the parabolic trough, the central receptor, and the parabolic dish [6]. Cost is, however, a key factor restricting the improvement of the PTC scheme. This problem will in part be alleviated by developing the thermal operation of the PTC method. Nanofluid has demonstrated a decent capacity to improve solar systems performance.

This specific liquid has been predicted as a topic of intensive global research by the extraordinary thermo and flow properties of nanofluid in comparison to traditional thermo transportation media. These powerful nanofluids work well with improved thermal conductance in lower concentrations of nanoparticles. It is also helpful in biomedical processing, soldering, lubrication, power systems, satellites, aeronautical devices, and thermal coordination for vehicles. Many authors are widely engaged in the application of nanomaterials to increase heat transfer. Conventional heat transfer rates cannot be obtained due to their inherently poor thermal conductance

under improved heat flux conditions. Over the last decade, the new approach of optimizing heat transfer by the application of ultrafine rigid particles in fluids has been widely explored. Choi [7] also introduced the term nanofluid to evaluate the thermal suspension in the base fluid with a higher precision through the dissemination of such nanosized solid particles. Early researches of nanofluids with a diversity of base fluids (propylene glycol (PG), H_2O, oils, etc.), calculated viscidness, thermal conductance, and observed that these nanofluid attributes were improved concerning the based fluids [8–12]. Apart from the thermal conductance and viscidness, the electric conductance of nano-solid particles (Cu, Ag, Au, CuO, ZnO, SiO_2, Fe_3O_4, Al_2O_3, TiO_2, CNT, etc.) and spread over many based liquids (H_2O, PG, Palm Oil, Coconut Oil, etc.) has been investigated for varying temperature ranges at different fractional sizes of these particles [13–15].

There has been a wide variety of research into modern nanofluid production; such liquids are referred to as hybrid nanofluid (HNF). Because of the combined impact of the interaction of multiple materials, HNFs boost their thermal properties. Jana and colleagues [16] first studied the hybridisation of various forms of nanoparticles to produce HNFs. The concept was to increase HNF thermal conductance over traditional nanofluids. This latest improvement is a conventional issue among researchers due to its possible benefits to nanofluids, results in the existence of several nanomolecules in the working liquid [17]. Many researchers have presumed that hybrid nanofluids or fused, mixed, or combined with two types of nanoparticles are present [18]. The concept to use HNFs is also to increase thermo-physical features, particularly the heat switch charge compared to regular nanofluids. Although the current type of nanoliquids is HNFs, their evaluation process is still in the improvement phase. High efficiency in terms of heat transfer can be expected by using HNFs [19]. Some nano-solid particles, including metal particles (Au, Al, Ag, Cu, and Fe), CNTs, and metallic oxides (Al_2O_3, TiO_2, CuO, SiC, and Fe_3O_4), were fascinated by the extensive groups of nanofluids [20]. Nanofluids offer unusual rheological results and thermo-physicochemical properties in different unit HNFs. Appropriate and satisfactory stability of the HNFs were appeared [21].

The use of renewable energy is a mechanism for overcoming the global energy crisis and plays a vital part in protecting the atmosphere against waste and emissions of all kinds of gases. Solar energy is also an integral basis of energy since the question is broadly posed to increase the accuracy of manufacturing technologies to improve organizational and environmental energy management [22, 23]. Linear Fresnel-reflectors (LFRs) are between the solar-collectors utilized for thermal converting solar-energy. Many works show that LFRs are an alternative approach that meets existing

energy needs [24-26]. Because of the poor thermal efficacy of the LFR, HNFs are a potential alternative for increasing the heat accuracy of the sample fluid by improving the thermal transfer functionality [27-34].

Entropy analysis is a valuable method to optimize thermal systems efficiency. The adding of nanomolecules to the standard liquid is known to affect the overall entropy generation. The use of nanofluids in thermal systems lowers the system temperature and ultimately reduces the contribution of the heat transfer to overall entropy production, thus added nanoparticles in the normal liquid upsurge the viscidness of the operating liquid leading to a reduction in the structure strain. Lots of studies have been studying entropy production to get optimal constraints for various thermally models and this is only covered by several articles. Sciacovelli et al. [35] for example, examined contributions to entropy-generation research theory and application to various systems of engineering. The second law analysis used for heater exchangers was used to interpret the examination of Manjunath and Kaushik [36]. Later on, Torabi et al. [37] were up-to-date in porous models for entropy production. In mono/hybrid nanofluids flow entropy production only an evaluation has been conducted in [38]. This evaluation includes an exhaustive study on entropy production in various geometries and flowing regimes

Solar radiations has been considered a heat source. The thermal transmission efficacy of the wings is analyzed for the status of diverse influences like thermal radiative flowing, heat generation, variant thermal conductance, and viscous dissipative flowing. Entropy production scrutiny has been carried out in the situation of RPNF. The modeled equations in terms of momentum and energy have been handled by Keller box technique (KBT). The effect of various potential factors on flow speed, shear-stress, and energy fields over and above frictional force coefficient and Nusselt number are discussed briefly and displayed in terms of figures and tables.

2. Model Formulations

The relationship of RPNF stress deformation [39] is presented as:

$$\frac{\partial u}{\partial y} = \frac{\tau}{\mu_\infty + \frac{\mu_0 - \mu_\infty}{1+\left(\frac{\tau}{\tau_s}\right)^2}}. \tag{1}$$

We consider

$$f(\sigma) = \frac{\sigma}{1+\frac{\lambda-1}{1+\sigma^2}}, \tag{2}$$

where $\sigma = \frac{\tau}{\tau_s}$ and $\lambda = \frac{\mu_0}{\mu_\infty}$.

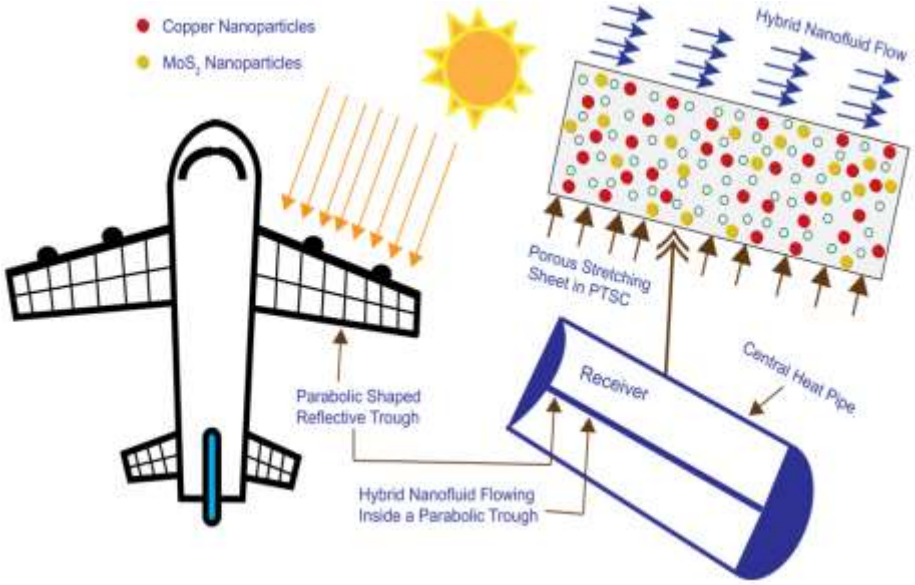

Fig. 1. Simulation of SACW.

Fig. 1 is demonstrated to study the mechanism of heat transport analysis of SACW. Solar radiations fall on the surface of the wings. Radiations penetrated through the wings and scatters on the parabolic through. The PTSC is stretching along $x - axis$ with Cu-MoS_2/EO type nanofluid flow over the trough surface. Engine oil is considered a base fluid. The symbols like T_w and T_∞ represents wall as well ambient temperatures respectively. μ_{hnf}, ρ_{hnf}, k_{hnf} and $(C_p)_{hnf}$ indicates dynamical viscidness, consistency, thermal conductance, and heat capacitance of HNF. Thermophysical features of utilized nanomolecules and base-liquid are demonstrated in Table 1. Fig. 2 represents the diagram planning of the given archetypal.

The controlling formulas regarding the continuity, impetus, and temperature [39] are given in component form as

$$\frac{\partial u}{\partial x} + \frac{\partial v}{\partial y} = 0, \tag{3}$$

$$u\frac{\partial u}{\partial x} + v\frac{\partial u}{\partial y} = \frac{\mu_{hnf}}{\rho_{hnf}}\frac{\partial \tau}{\partial y} - \frac{\mu_{hnf}}{K\rho_{hnf}}u, \tag{4}$$

$$u\frac{\partial T}{\partial x} + v\frac{\partial T}{\partial y} = \frac{\partial}{\partial y}\left(\frac{k_{hnf}}{(\rho C_p)_{hnf}}\frac{\partial T}{\partial y}\right) - \frac{1}{(\rho C_p)_{hnf}}\frac{\partial q_r}{\partial y} + \frac{\mu_{hnf}}{\rho C_p)_{hnf}}\left(\frac{\partial u}{\partial y}\right)^2 + \frac{Q_0(T-T_\infty)}{(\rho C_p)_{hnf}}, \tag{5}$$

with

$$\left.\begin{aligned} &y = 0 \quad : \quad u = ax^{\frac{1}{3}},\ v = 0,\ T = T_w, \\ &y \to \infty: \quad u \to 0,\ T \to T_\infty. \end{aligned}\right\} \tag{6}$$

Then we consider [40]:

$$\left.\begin{aligned} &\rho_{nf} = (1-\phi)\rho_f + \phi\rho_s, \\ &\mu_{nf} = \frac{\mu_f}{(1-\phi)^{2.5}}, \\ &(\rho C_p)_{nf} = (1-\phi)(\rho C_p)_f + \phi(\rho C_p)_s, \\ &\frac{k_{nf}}{k_f} = \left[\frac{(k_s+(m-1)k_f)-(m-1)\phi(k_f-k_s)}{(k_s+(m-1)k_f)+\phi(k_f-k_s)}\right], \end{aligned}\right\} \tag{7}$$

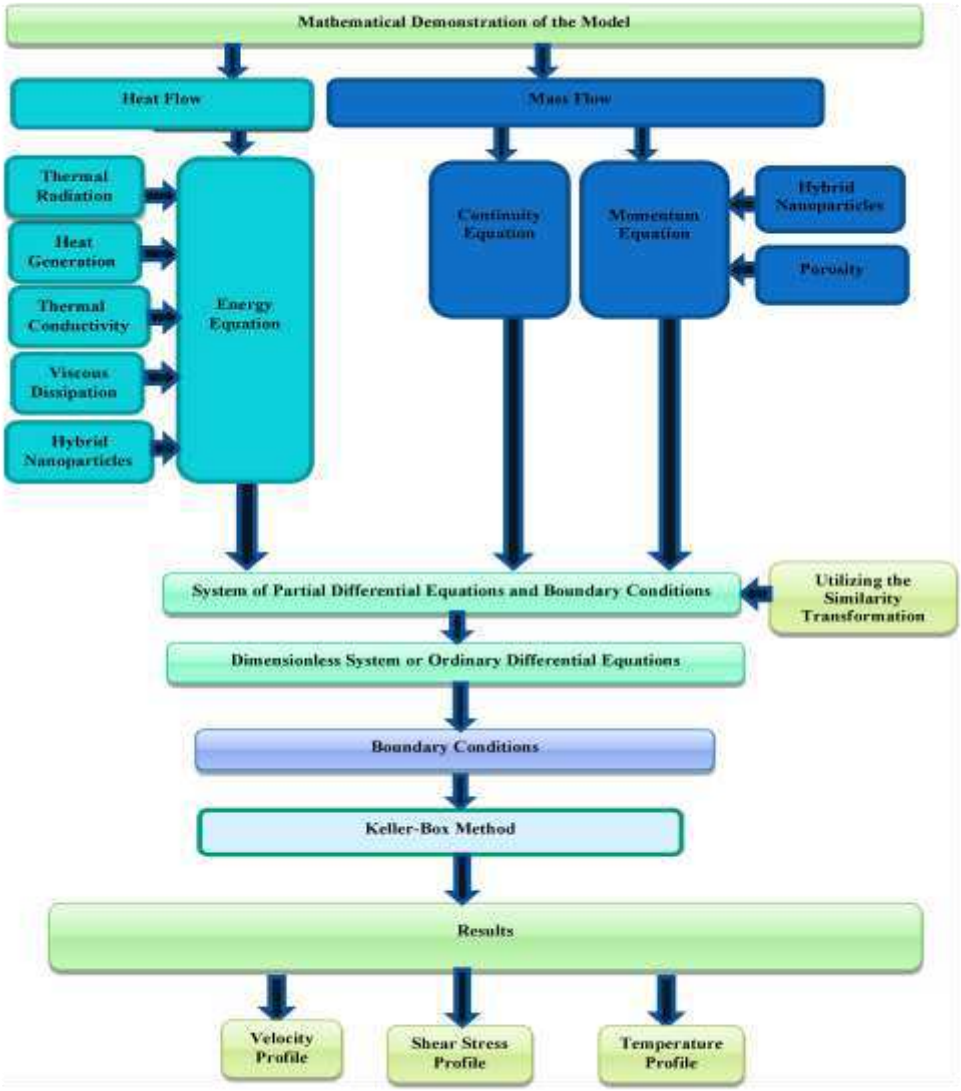

Fig. 2. Simulation of the model.

Then we construct [12, 18]:

$$\left.\begin{aligned}
&\mu_{hnf} = \frac{\mu_f}{(1-\phi_1)^{2.5}(1-\phi_2)^{2.5}},\\
&\rho_{nf} = [(1-\phi_1)\rho_f + \phi_1\rho_{s_1}](1-\phi_2) + \phi_2\rho_{s_2},\\
&(\rho C_p)_{hnf} = (1-\phi_2)[\phi_1(\rho C_p)_{s_1} + (1-\phi_1)(\rho C_p)_f] + \phi_2(\rho C_p)_{s_1},\\
&\frac{k_{nf}}{k_f} = \left[\frac{(k_{s_2}+(m-1)k_f)-(m-1)\phi_2(k_f-k_{s_2})}{(k_{s_2}+(m-1)k_f)+\phi_2(k_f-k_{s_2})}\right]\times\\
&\qquad\left[\frac{(k_{s_1}+(m-1)k_f)-(m-1)\phi_1(k_f-k_{s_1})}{(k_{s_1}+(m-1)k_f)+\phi_1(k_f-k_{s_1})}\right],
\end{aligned}\right\} \tag{8}$$

Table 1. Thermophysical features.

Features	Engine Oil (EO)	Copper (Cu)	(MoS_2)
ρ	884	8933	5060
C_p	1910	385	397.21
k	0.144	401	904.4

Then, we get

$$q_r = -\frac{4\sigma^*}{3\kappa^*}\frac{\partial T^4}{\partial y}, \tag{9}$$

and

$$\psi = \sqrt{U(x)xv}f(\eta), \eta = \sqrt{\frac{U(x)}{vx}}y, \tau = \rho\sqrt{U_0^3 v}g(\eta), \theta(\eta) = \frac{T-T_\infty}{T_0-T_\infty}, \tag{10}$$

Thus, we reach

$$g' = \frac{1}{3A_1A_2}f'^2 - \frac{2}{3}ff'' - \lambda_1 f', \tag{11}$$

$$g = f''\frac{g^2+\lambda\gamma^2}{g^2+\gamma^2}, \tag{12}$$

$$\left\{\left[(1+\epsilon)+\frac{Rd}{A_4}\right]\theta'' + \epsilon\theta'^2\right\} + \frac{2}{3}\frac{A_3}{A_4}Prf\theta' + \frac{A_1}{A_4}\ Pr\ \ Ec\ \ f''^2 + \frac{Q}{A_4}\theta = 0, \tag{13}$$

with

$$\left.\begin{aligned}
&\eta = 0 \quad : f(\eta) = 0, \qquad f'(\eta) = 1, \qquad \theta'(0) = 1,\\
&\eta \to \infty : f'(\eta) \to 0, \qquad \theta(\eta) \to 0.
\end{aligned}\right\} \tag{14}$$

Finally, we obtain

$$\left.\begin{aligned}
&\gamma = \left(\frac{\tau_s}{\rho\sqrt{U_0^3 v}}\right), \lambda = \frac{\mu_0}{\mu_\infty},\ Pr = \frac{\mu C_p}{k_\infty}, R_d = \frac{16\sigma T_\infty^3}{3k^*k_\infty},\ \lambda = \frac{v}{Ka},\\
&Ec = \frac{u_w}{Cp(T_0-T_\infty)},\ Q = \frac{Q_0(T_0-T_\infty)}{(\rho C_p)_{hnf}}.
\end{aligned}\right\} \tag{15}$$

We have

$$Cf_x = \frac{\tau_w}{\rho u_w^2}, \qquad Nu_x = \frac{x q_w}{k_f(T_w - T_\infty)}, \tag{16}$$

and

$$\tau_w = \mu_{hnf}\tau, \; q_w = -\left[k_{hnf} + \frac{16\sigma^*}{3\kappa^*}T_\infty^3 \frac{\partial T}{\partial y}\right]. \tag{17}$$

Nonimensional formula of frictional force is demonstrated as:

$$Cf_x Re_x^{1/2} = \frac{g}{A_1}, \tag{18}$$

The nondimensional Nusselt number is presented as:

$$Nu_x Re_x^{-1/2} = -A_4(1 + Rd)\theta' \tag{19}$$

whereas A_1, A_2, A_3 and A_4 are given by

$$\left.\begin{aligned} A_1 &= \frac{1}{(1-\phi_1)^{2.5}(1-\phi_2)^{2.5}}, \\ A_2 &= [(1-\phi_1) + \phi_1 \frac{\rho_{s_1}}{\rho_f}](1-\phi_2) + \phi_2 \frac{\rho_{s_2}}{\rho_f}, \\ A_3 &= (1-\phi_2)[\phi_1 \frac{(\rho C_p)_{s_1}}{\rho C_p)_f}) + (1-\phi_1)] + \phi_2 \frac{(\rho C_p)_{s_2}}{\rho C_p)_f}, \\ A_4 &= \left[\frac{(k_{s_2}+(m-1)k_f)-(m-1)\phi_2(k_f-k_{s_2})}{(k_{s_2}+(m-1)k_f)+\phi_2(k_f-k_{s_2})}\right] \times \\ &\quad \left[\frac{(k_{s_1}+(m-1)k_f)-(m-1)\phi_1(k_f-k_{s_1})}{(k_{s_1}+(m-1)k_f)+\phi_1(k_f-k_{s_1})}\right], \end{aligned}\right\} \tag{20}$$

Table 2 shows comparing of the consequences with Ref. [41] for diverse values of γ.

Table 2. Comparing of the consequences with Ref. [41].

$Nu_x Re_x^{\frac{-1}{2}}$ (Absent Rd)				
	$\lambda = 0.5$		$\lambda = 1$	
γ	Current	Reddy [41]	Current	Reddy [41]
0.1	0.130909	0.109782	0.144535	0.114058
0.2	0.109284	0.102621	0.144535	0.114058
0.3	0.085161	0.097438	0.144535	0.114058

3. Numerical Procedure

Fig. 3 shows the procedure diagram of the numerical KBT.

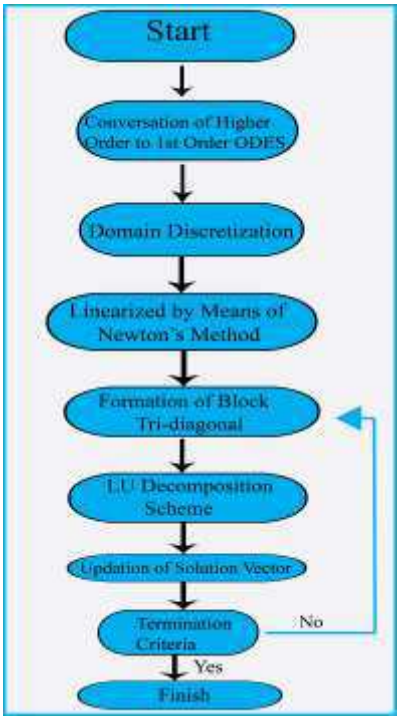

Fig. 3. KBT diagram.

We have

$$\frac{df}{d\eta} = u_1, \tag{21}$$

$$\frac{d\tilde{u}_1}{d\eta} = u_2, \tag{22}$$

$$\frac{d\theta}{d\eta} = u_3, \tag{23}$$

$$\frac{du_2}{d\eta} - \frac{g^2+r^2}{g^2+\lambda r^2}\left[\frac{1}{A_1A_2}u_1^2 - \frac{2}{3}fu_2 - \lambda_1 u_1\right] = 0, \tag{24}$$

and

$$\left((1+\epsilon) + \frac{Rd}{A_4}\right)\frac{du_3}{d\eta} + \epsilon u_3^2 + \frac{2A_3}{3A_4}Prfu_3 + PrEc\frac{A_1}{A_4}u_2^2 + \frac{Q}{A_4}\theta = 0. \tag{25}$$

$$\left.\begin{aligned} &f(0) = 0, u_1(0) = 1, u_3(0) = 1, \\ &u_1 \to 0, \quad \theta \to 0 \quad \text{as} \quad \eta \to \infty. \end{aligned}\right\} \tag{26}$$

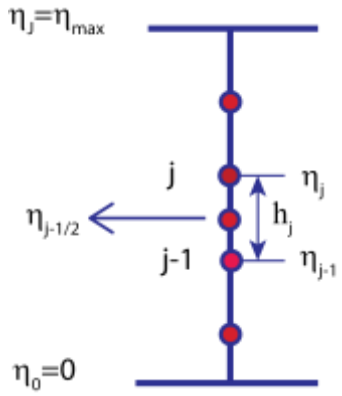

Fig. 4. Domain discretization.

We have

$$\eta_0 = 0, \qquad \eta_j = \eta_{j-1} + h_j,\ j = 0,1,2,3\ldots,J, \qquad \eta_J = \eta_\infty$$ where, h_j is the step-size (Fig. 4). Then, we reach

$$\frac{f_j - f_{j-1}}{h_j} - \frac{(u_1)_j + (u_1)_{j-1}}{2} = 0, \tag{27}$$

$$\frac{(u_1)_j - (u_1)_{j-1}}{h_j} - \frac{(u_2)_j + (u_2)_{j-1}}{2} = 0, \tag{28}$$

$$\frac{\theta_j - \theta_{j-1}}{h_j} - \frac{(u_3)_j + (u_3)_{j-1}}{2} = 0, \tag{29}$$

$$\left.\begin{aligned} &((u_2)_j - (u_2)_{j-1}) - \frac{h_j}{2}\frac{g^2+r^2}{g^2+\lambda r^2}\left[\frac{1}{3A_1A_2}\left(\frac{(u_1)_j + (u_1)_{j-1}}{2}\right)^2\right] + \frac{h_j}{2}\frac{g^2+r^2}{g^2+\lambda r^2} \\ &\lambda_1\left(\frac{(u_1)_j + (u_1)_{j-1}}{2}\right) + \frac{h_j}{3}\frac{g^2+r^2}{g^2+\lambda r^2}(f_j + f_{j-1})((u_1)_j + (u_1)_{j-1}) = 0 \end{aligned}\right\}, \tag{30}$$

$$\left.\begin{aligned} &((1+\epsilon) + \frac{Rd}{A_4})((u_3)_j - (u_3)_{j-1}) + \epsilon h_j\left(\frac{(u_3)_j + (u_3)_{j-1}}{2}\right)^2 \\ &+ \frac{2h_jA_3Pr}{3A_4}\left(\frac{f_j + f_{j-1}}{2}\right)\left(\frac{(u_3)_j + (u_3)_{j-1}}{2}\right) \\ &+ \frac{h_jPrEcA_1}{A_4}\left(\frac{(u_2)_j + (u_2)_{j-1}}{2}\right)^2 + h_j\frac{Q}{A_4}\left(\frac{\theta_j + \theta_{j-1}}{2}\right) = 0. \end{aligned}\right\} \tag{31}$$

The nonlinearity formulas (28)-(32) structure should be linearized by the Newton method. We have

$$\left.\begin{aligned} &f_j^{n+1} = f_j^n + \delta f_j^n, \qquad (u_1)_j^{n+1} = (u_1)_j^n + \delta(u_2)_j^n, \qquad (u_2)_j^{n+1} = (u_2)_j^n + \delta(u_2)_j^n, \\ &(u_3)_j^{n+1} = (u_3)_j^n + \delta(u_3)_j^n, \qquad \theta_j^{n+1} = \theta_j^n + \delta\theta_j^n. \end{aligned}\right\} \tag{32}$$

Then, we obtain

$$\delta f_j - \delta f_{j-1} - \frac{h_j}{2}(\delta(u_1)_j + \delta(u_1)_{j-1}) = (r_1)_j, \tag{33}$$

$$\delta(u_1)_j - \delta(u_1)_{j-1} - \frac{h_j}{2}(\delta(u_2)_j + \delta(u_2)_{j-1}) = (r_2)_j, \tag{34}$$

$$\delta\theta_j - \delta\theta_{j-1} - \frac{h_j}{2}(\delta(u_3)_j + \delta(u_3)_{j-1}) = (r_3)_j, \tag{35}$$

$$(a_1)_j\delta f_j + (a_2)_j\delta f_{j-1} + (a_3)_j\delta(u_1)_j + (a_4)_j\delta(u_1)_{j-1} + (a_5)_j\delta(u_2)_j + (a_6)_j\delta(u_2)_{j-1} = (r_4)_j, \tag{36}$$

$$(b_1)_j\delta f_j + (b_2)_j\delta f_{j-1} + (b_3)_j\delta(u_2)_j + (b_4)_j\delta(u_2)_{j-1} + (b_5)_j\delta(u_3)_j + (b_6)_j\delta(u_3)_{j-1} + (b_7)_j\delta\theta_j + (b_8)_j\delta\theta_{j-1} = (r_5)_j, \tag{37}$$

where

$$\left.\begin{aligned}
&(a_1)_j = \frac{2h_j}{3}\frac{g^2+r^2}{g^2+\lambda r^2}\frac{((u_2)_j+(u_2)_{j-1})}{4}, \qquad (a_2)_j = (a_1)_j,\\
&(a_3)_j = \frac{h_j\lambda_1}{2}\frac{g^2+r^2}{g^2+\lambda r^2} - \frac{h_j}{3A_1A_2}\frac{g^2+r^2}{g^2+\lambda r^2}\frac{((u_1)_j+(u_1)_{j-1})}{2} = (a_4)_j,\\
&(a_5)_j = 1 + \frac{2h_j}{3}\frac{g^2+r^2}{g^2+\lambda r^2}\frac{(f_j+f_{j-1})}{4} = (a_6)_j,\\
&(r_4)_j = -\frac{h_j\lambda_1}{2}\frac{g^2+r^2}{g^2+\lambda r^2}((u_1)_j + (u_1)_{j-1}) + \frac{h_j}{12A_1A_2}\frac{g^2+r^2}{g^2+\lambda r^2}((u_1)_j + (u_1)_{j-1})^2\\
&-\frac{h_j}{6}\frac{g^2+r^2}{g^2+\lambda r^2}(f_j + f_{j-1})((u_2)_j + (u_2)_{j-1}) - ((u_2)_j - (u_2)_{j-1}),
\end{aligned}\right\} \tag{38}$$

$$\left.\begin{aligned}
&(b_1)_j = \frac{2h_jPrA_3}{3A_4}\frac{((u_3)_j+(u_3)_{j-1})}{4}, \qquad (b_2)_j = (b_1)_j,\\
&(b_3)_j = \frac{h_jPrA_1Ec}{A_4}\frac{((u_2)_j+(u_2)_{j-1})}{2}, \qquad (b_4)_j = (b_3)_j,\\
&(b_5)_j = ((1+\epsilon) + \frac{Rd}{A_4}) + \frac{2h_jPrA_3}{3A_4}\frac{(f_j+f_{j-1})}{4} + \epsilon h_j\frac{((u_3)_j+(u_3)_{j-1})}{2},\\
&(b_6)_j = -((1+\epsilon) + \frac{Rd}{A_4}) + \frac{2h_jPrA_3}{3A_4}\frac{(f_j+f_{j-1})}{4} + \epsilon h_j\frac{((u_3)_j+(u_3)_{j-1})}{2},\\
&(b_7)_j = \frac{1}{2}\frac{h_jQ}{A_4} = (b_8)_j,\\
&(r_6)_j = -((1+\epsilon) + \frac{Rd}{A_4})((u_3)_j - (u_3)_{j-1}) - \epsilon h_j(\frac{(u_3)_j+(u_3)_{j-1}}{2})^2\\
&-\frac{2h_jA_3Pr}{3A_4}(\frac{f_j+f_{j-1}}{2})(\frac{(u_3)_j+(u_3)_{j-1}}{2})\\
&-\frac{h_jPrEcA_1}{A_4}(\frac{(u_2)_j+(u_2)_{j-1}}{2})^2 - h_j\frac{Q}{A_4}(\frac{\theta_j+\theta_{j-1}}{2}).
\end{aligned}\right\} \tag{39}$$

Then, we get

$$A\delta = R, \tag{40}$$

where

$$A = \begin{bmatrix} [A_1] & [C_1] & & & & & \\ & [A_2] & [C_2] & & & & \\ & & \ddots & & & & \\ & & & \ddots & & & \\ & & & & \ddots & & \\ & & & & [B_{J-1}] & [A_{J-1}] & [C_{J-1}] \\ & & & & & [B_J] & [A_J] \end{bmatrix}, \delta = \begin{bmatrix} [\delta_1] \\ \vdots \\ \vdots \\ \vdots \\ \\ \end{bmatrix} \text{ and } \quad R = \begin{bmatrix} [R_1] \\ \vdots \\ \vdots \\ \vdots \\ \\ \end{bmatrix}.$$

where the elements defined in Eq. (38) are

$$[A_1] = 3pt \begin{bmatrix} 0 & 0 & 1 & 0 & 0 \\ -0.5h_1 & 0 & 0 & -0.5h_1 & 0 \\ 0 & -0.5h_1 & 0 & 0 & -0.5h_1 \\ (a_6)_1 & 0 & (a_1)_1 & (a_5)_1 & 0 \\ (b_4)_1 & (b_6)_1 & (b_1)_1 & (b_3)_1 & (b_5)_1 \end{bmatrix},$$

$$[A_j] = 3pt \begin{bmatrix} -0.5h_j & 0 & 1 & 0 & 0 \\ -1 & 0 & 0 & -0.5h_j & 0 \\ 0 & -1 & 0 & 0 & -0.5h_j \\ (a_4)_j & 0 & (a_1)_j & (a_5)_j & 0 \\ 0 & (b_8)_j & (b_1)_j & (b_3)_j & (b_5)_j \end{bmatrix}, 2 \le j \le J$$

$$[B_j] = 10pt \begin{bmatrix} 0 & 0 & -1 & 0 & 0 \\ 0 & 0 & 0 & -0.5h_j & 0 \\ 0 & 0 & 0 & 0 & -0.5h_j \\ 0 & 0 & (a_2)_j & (a_6)_j & 0 \\ 0 & 0 & (b_2)_j & (b_4)_j & (b_6)_j \end{bmatrix}, 2 \le j \le J$$

$$[C_j] = 8pt \begin{bmatrix} -0.5h_j & 0 & 0 & 0 & 0 \\ 1 & 0 & 0 & 0 & 0 \\ 0 & 1 & 0 & 0 & 0 \\ (a_3)_j & 0 & 0 & 0 & 0 \\ 0 & (b_7)_j & 0 & 0 & 0 \end{bmatrix}, 1 \le j \le J-1.$$

Factorizing A as

$$A = LU, \tag{41}$$

where

$$L=\begin{bmatrix}[\alpha_1] & & & & \\ & [\alpha_2] & & & \\ & & \ddots & & \\ & & \ddots & [\alpha_{J-1}] & \\ & & & [B_J] & [\alpha_J]\end{bmatrix}, U=\begin{bmatrix}[I] & [b_1] & & & \\ & [I] & [b_2] & & \\ & & \ddots & \ddots & \\ & & & [I] & [b_{J-1}] \\ & & & & [I]\end{bmatrix},$$

here $[I]$ signfies the unity matrix with O(5), $[\alpha_i]$, $[B_i]$ and $[b_i]$ are 5×5 matrices. We have

$$E_{\mathrm{g}}=\frac{k_{nf}}{T_\infty^2}\left(\left(\frac{\partial T}{\partial y}\right)^2+\frac{16\sigma^* T_\infty^3}{3\kappa^*}\left(\frac{\partial T}{\partial y}\right)^2\right)+\frac{\mu_{nf}}{T_\infty}\left(\frac{\partial u}{\partial y}\right)^2+\frac{\mu_{nf}}{T_\infty}u^2, \tag{42}$$

and

$$N_{\mathrm{g}}=\frac{T_\infty^2 a^2 E_G}{\kappa_f(T_w-T_\infty)^2}, \tag{43}$$

the dimensionless expression regarding entropy generation is bestowed by

$$N_{\mathrm{g}}=Re\left(A_4(1+Rd)\theta'^2+\frac{1}{A_1}\frac{Br}{\Omega}(f''^2+\lambda_1 f'^2)\right). \tag{44}$$

4. Results and Discussions

Figs. 5-8 design to reverberate the performance of RPNF parameter λ on the velocites $f'(\eta)$, $g(\eta)$, and temperature $\theta(\eta)$ and entropic production N_{g}. The viscosity of the fluid debacles by the virtue of an amplification in λ which contribute towards the minimization of fluid viscosity and speed of the nanofluid as well. It is quite interesting that the shear stress of the fluid lessens for the case an augmentation in λ consequently diminishes $g(\eta)$. It is observed that the viscosity of the fluid diminishes by amplifying fluid temperature and the fluid behaves like shear thinning which improves the temperature phenomenon of the fluid $\theta(\eta)$. An amplification in temperature means the fluid particles possess enormous kinetic energy. It means that the particles moving faster brings about more disorder in comparison to particles in fluid moving with lower speed. Thats why an embellishment in temperature booms entropy N_{g}. It is also observed that the hybrid nanoparticles particles amplifies temperature and entropy much better in contrast to the simple nanofluid.

Figs. 9-12 sway the impact of Bingham factor γ on $f'(\eta)$, $g(\eta)$, $\theta(\eta)$ and N_{g}. Bingham number is the ratio between yield stress as well as viscidness-stress. All of λ and γ are essential factors of RPNF and almost behaves in a same manner. It is noted that a enlargement in viscidness lessens the yield-stress and improves γ and furthermore behaves like shear-thinning. As a result a shear thinning phenomenon, the fluid flow over the surface which amplifies the velocity and shea stress domain. Viscidness of the nanofluid depreciates on the account of magnification in γ. The

temperature phenomenon is contrarywise associated to the nanofluid viscosity. Decremental change in nanofluid viscidness drives to a enlargement in the fluid temperature. Global the entropic rate of the nanofluid booms due to an amplification in the temperature phenomenon.

The effect of Reynold Re, Brinkman Br numbers and Ω on entropic production N_g is highlighted in Figs. 13-15. It is quite clear that the viscous forces becomes less dominant as compared to inertial forces in the status of an augmentation variation in Re. As a result of inertial forces dominance over viscous produces a magnification in temperature which elevates N_g. The relation between Br and N_g is highlighted in Fig. 14. Brinkman number Br can be defined as heat dissipation to the conduction. It is noted that the considerable heat is dissipated on the account of an increment in Br elevates entropy of the system. The impact of dimensionless temperature variations Ω on N_g is displayed in Fig. 15. It is observed that the heat dissipation process amplifies on the account of an amplification in Ω which diminishes N_g. The effect of porosity parameter λ_1 on $f'(\eta)$, $g(\eta)$, $\theta(\eta)$ and N_g is emphasized in Figs. 16-18.

Figs. 19 and 20 reflect the impact of thermal conductance ϵ. When molecules of the fluid collides more randomly exchange much kinetic energy with each other in comparison to normal collision which eventually produces much heat inside the fluid. On other hand due to this frequent collision of the molecules the temperature of the fluid amplifies which augments temperature field and entropy $\theta(\eta)$ and N_g.

Fig. 21 and 22 reflects the influence of Prandtl number Pr on $\theta(\eta)$ and N_g. Thermal conductance of the nanofluid debacles in the status of a amplification in Pr which lessens the temperature of the fluid as well. Prandtl is impetus diffusion to thermal diffusion. Impetus diffusion predominants thermal diffusion which brings about a decrement in temperature. Thermal boundary thickness decreases and decreases more in the case of N_g.

Figs. 23 and 24 are designed to reveal the impact of Eckert number Ec on the heat field $\theta(\eta)$ and entropic production. The parameter Ec is actually kinetical energy to enthalpic variance. A positive variation in kinetical energy enhances heat transfer phenomenon. Nanomolecules shock extra at random due to a development in the kinetic energy. Internal heat generation capacity of the fluid improves by the virtue of an amplification in Ec. The PTSC transports heat more effectively within SACW because of a variation of Ec values. When solar thermal radiations fall on the trough present in the wing, the nanoparticles present on the trough surface collides more frequently and

heating capacity of the trough improves and distribute heat quite effectively inside the wings and other parts of the aircraft. generation capacity of the fluid. From this figure, the mixture nanomolecules delivers well the heat in contrast to simple nanofluid.

Internal heat generation Q and Rd on $\theta(\eta)$ and N_g are emphasized in Figs. 25-28. Thermal boundary thickness along with the heat transmission of the hybrid-nanofluid is better in contrast to simple nanofluid. A positive change in Q generates more inside the fluid which improves thermal transport process of the nanofluid. When solar radiations fall on the surface of the parabolic trough. The internal heat generation capacity of the trough improves and provides extensive heat to the nanoparticles based fluid. The heat delivers effectively in the situation of mixture nanomolecules based liquid in contrast to the natural base fluid. Radiations are the main source of heat energy. Solar thermal radiations have change the whole concept of the renewable energy and provides different ideas to the researchers to work on the ideas of solar air craft wings, solar water pumps, solar motor bikes etc. When these solar radiations continuously fall on the surface of the trough, it delivers extensive to the nanoliquid flowing over PTSC. Thermal conduction process of the fluid improves in the case of magnification in Rd which elevates temperature phenomenon. The heat besides total entropic rate of the model improves owing to a magnification in Rd and heat generation Q.

The effect of volume fractions of nanoparticles ϕ_{hnf} on flowing speed $f'(\eta)$, shear-stress $g(\eta)$, temperature $\theta(\eta)$ fields and entropic production N_g are highlighted in Figs. 29-32. The concentration of the nanoparticles amplifies on the behalf of an benefication in ϕ_{hnf} which elevates the velocity field. The inertial forces dominate viscous forces which diminishes the shear stress behaviour of the fluid and moreover $g(\eta)$. The augmentation in size of nanomolecules enhances thermal conductance over and above the rate of heat transport of the fluid. Insertion of nanomolecules in the normal liquid boosts heat conductance of the base liquid. Thickness of the thermal boundary layer in addition to the rate of heat transmission of the improves by the virtue of an augmentation in nanomolecules size. The solar radiations along with ϕ_{hnf} enhances the over all performance of parabolic trough surface collector and delivers heat effectively inside the air craft wings. Consequently $\theta(\eta)$ and N_g amplifies.

The effect of parameter m mention diverse forms of nanomolecules in the form of sphere having value $m = 3$, hexadron $= 3.7221$, tetrhedron $= 4.0613$ and column $= 6.3698$ on temperature $\theta(\eta)$ as well as N_g is depicted in Figs. 33 and 34. It is observed that an incremental

change in m improves temperature along with the rate of heat transport rate of the nanoliquid. Sphere occupy more space in comparison to other shapes of nanoparticles. The column shape nanoparticles 6.3698 produces much heat and temperature of the nanoparticles escalates in comparison to other shapes of nanoparticles. The column shape nanoparticles occupy less space in contrast to sphere. From figure it is quite clear that the thermal boundary thickness of the fluid improves in the case of vertical column in comparison to other shapes. A positive change in m and hybrid nanoparticles Cu-MoS_2 delivers considerable heat collect by the PTSC and transfer in through out the aircraft wing.

Table 3 is sketched to work the effect of many various variables on the frictional force coefficient C_f and the rate of heat transmission Nu in the situation of mixture nano-fluid and standard nano-fluid. The frictional force factor improves in the status of liquid factor λ nonetheless diminishes for Bingham number γ and porosity parameter λ_1. No change is reported for the case of remaining parameter. From this table the hybrid nanomolecules delivers well results in comparing to the standard nanoliquid. The thermal transfer rate improves in the case of λ, λ_1, variant thermal conductance ϵ, Prandtl number Pr, heat generation Q, thermal radiative flow Rd, nanomolecules form m, mixture nanofluid ϕ_{hnf} and nano-solid particles size of ϕ. These parameters elevates the performance of nanofluid flow over a PTSC present in SACW.

Table 4 reported the effect of energy parameters ϵ, Pr, Ec Q, Rd on the heat transfer for the situation of hybridity nanoliquid Cu-MoS_2/EO and simple nanoliquid Cu/EO. Error ratio depicts the difference between simple nanofluid and hybrid nanofluid in relation with heat transmission rate. The percentage rate of heat transmission of the Ec and Rd is greater 14.7% in comparison to other parameters value.

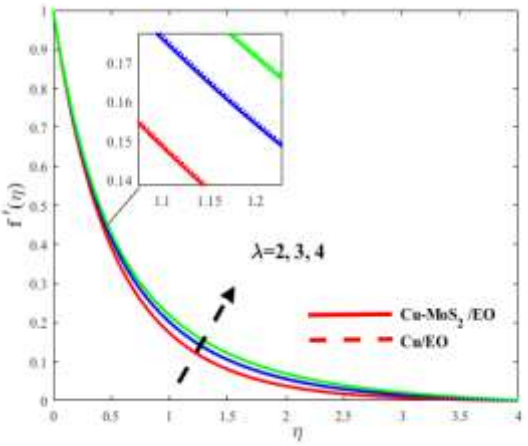

Fig. 5. Impression of λ on $f'(\eta)$.

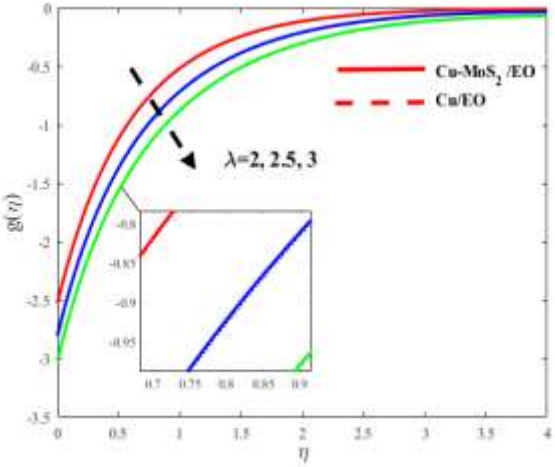

Fig. 6. Impression of λ on $g(\eta)$.

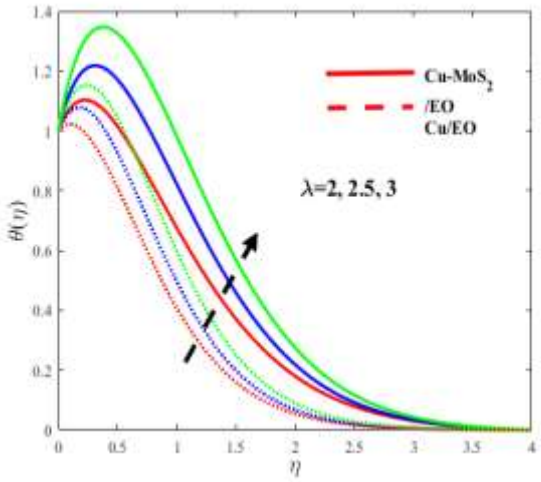

Fig. 7. Impression of λ on $\theta(\eta)$.

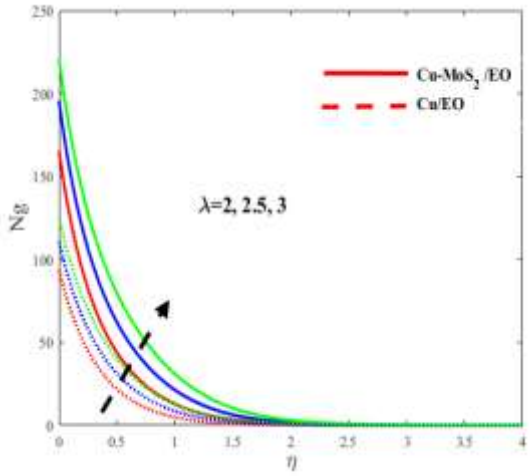

Fig. 8. Impression of λ on N_g.

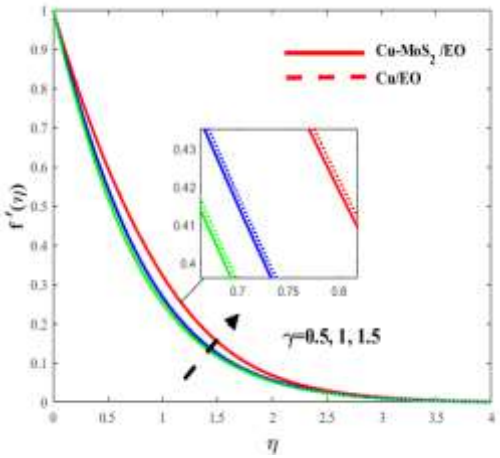

Fig. 9. Impression of γ on $f'(\eta)$.

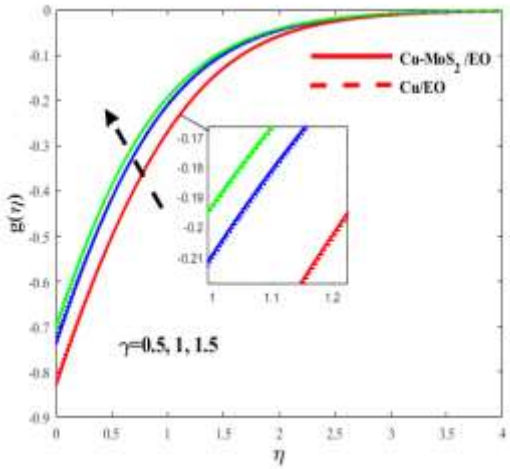

Fig. 10. Impression of γ on $g(\eta)$.

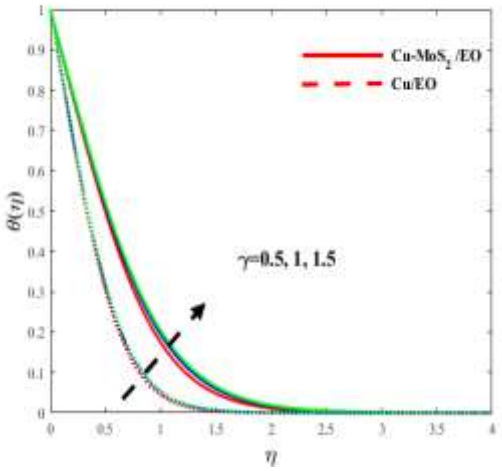

Fig. 11. Impression of γ on $\theta(\eta)$.

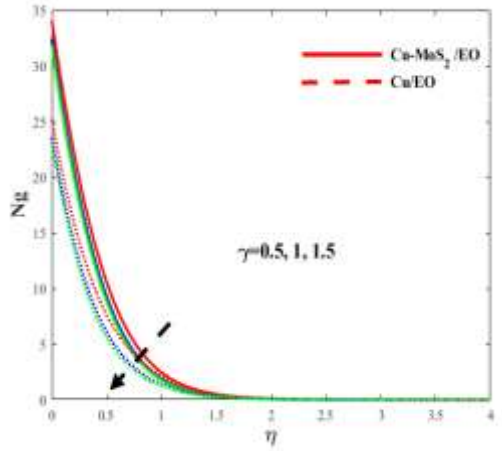

Fig. 12. Impression of γ on N_{g}.

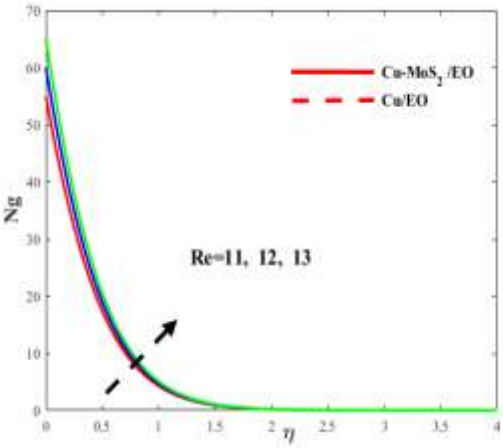

Fig. 13. Impression of Re on N_{g}.

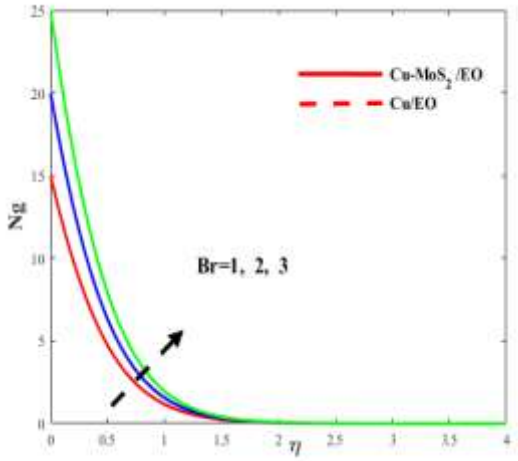

Fig. 14. Impression of Br on N_g.

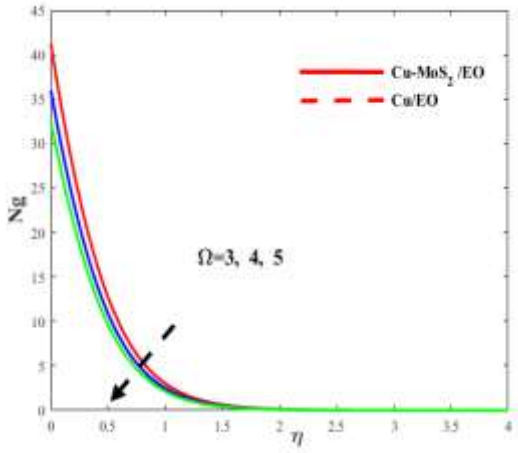

Fig. 15. Effect of Ω on N_g.

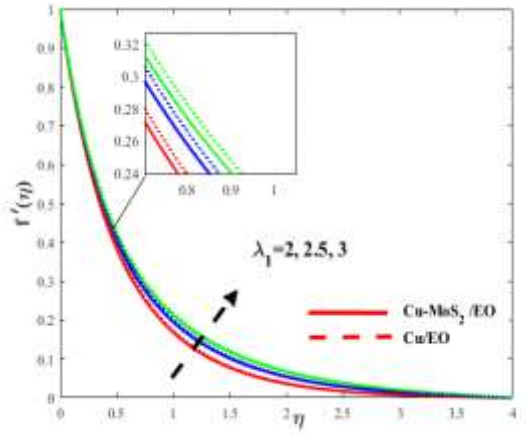

Fig. 16. Effect of λ_1 on $f'(\eta)$.

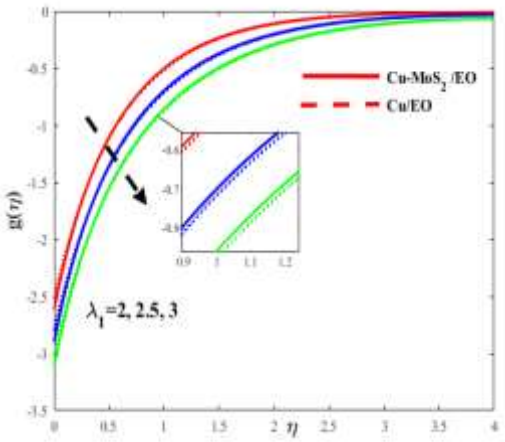

Fig. 17. Effect of λ_1 on $g(\eta)$.

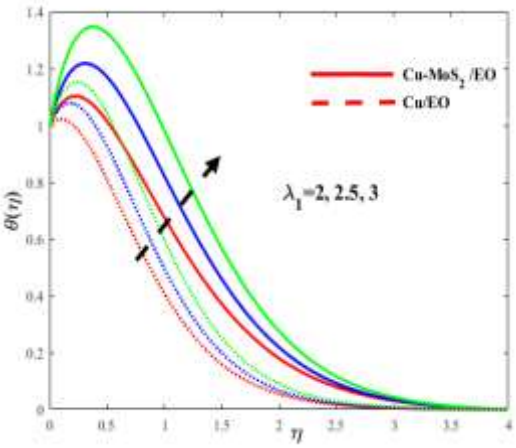

Fig. 18. Effect of λ_1 on $\theta(\eta)$.

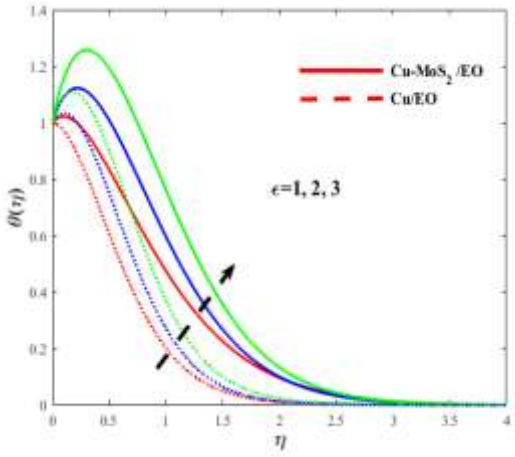

Fig. 19. Effect of ϵ on $\theta(\eta)$.

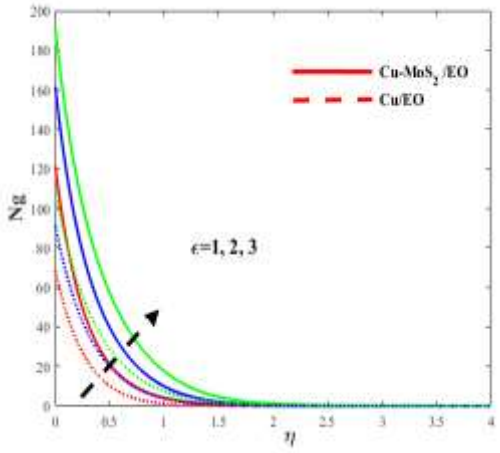

Fig. 20. Effect of ϵ on N_{g}.

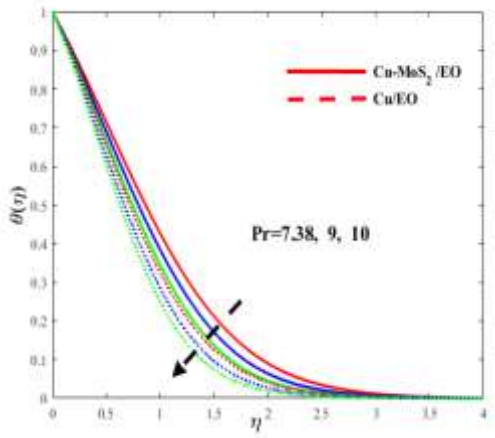

Fig. 21. Effect of Pr on $\theta(\eta)$.

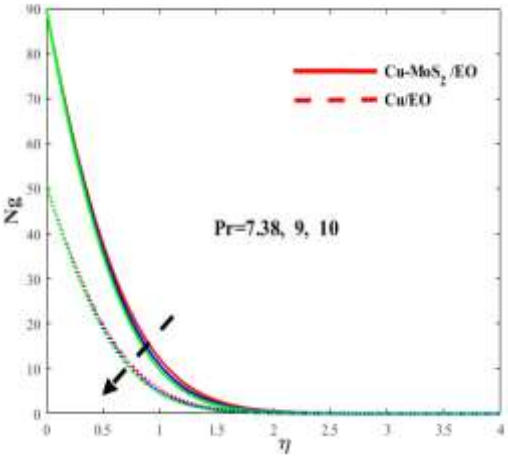

Fig. 22. Effect of Pr on N_{g}.

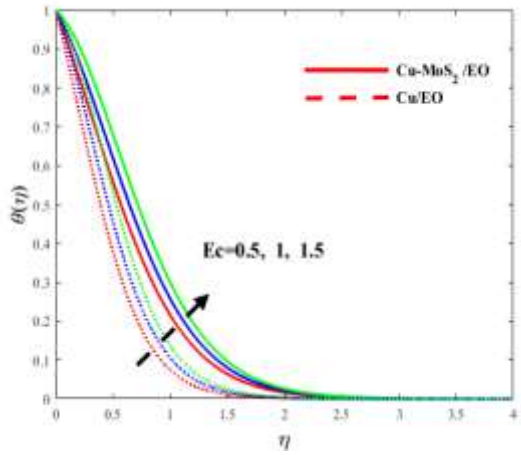

Fig. 23. Change of Ec on $\theta(\eta)$.

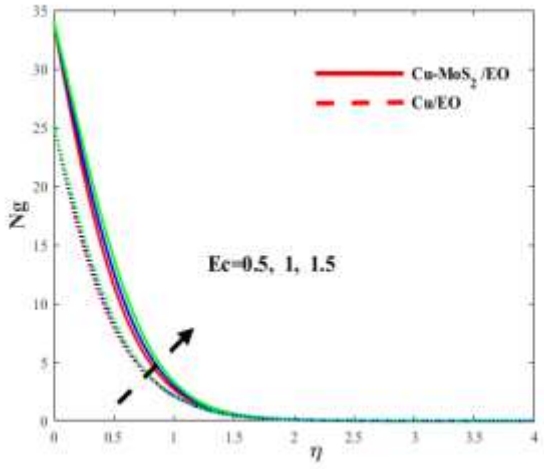

Fig. 24. Change of Ec on N_{g}.

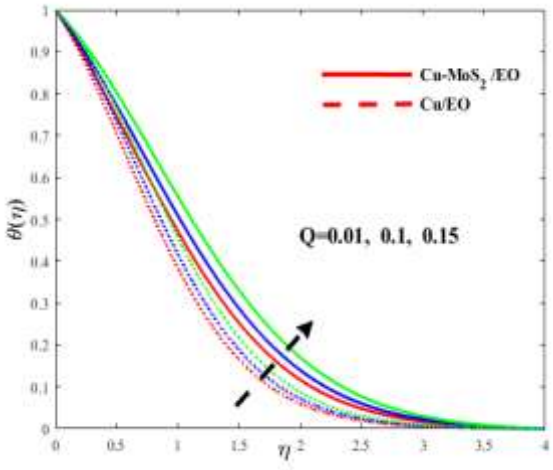

Fig. 25. Change of Q on $\theta(\eta)$.

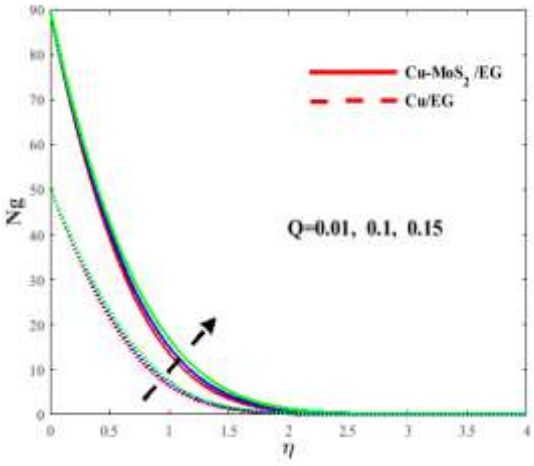

Fig. 26. Change of Q on N_g.

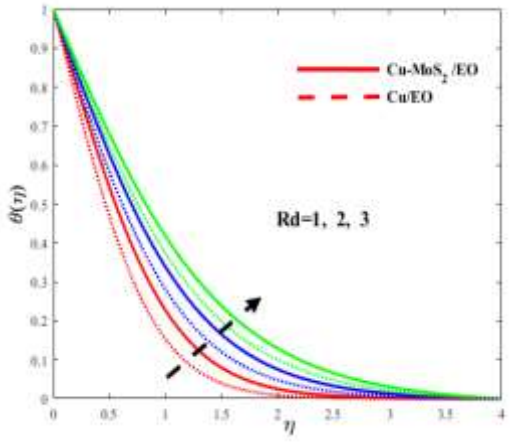

Fig. 27. Change of Rd on $\theta(\eta)$.

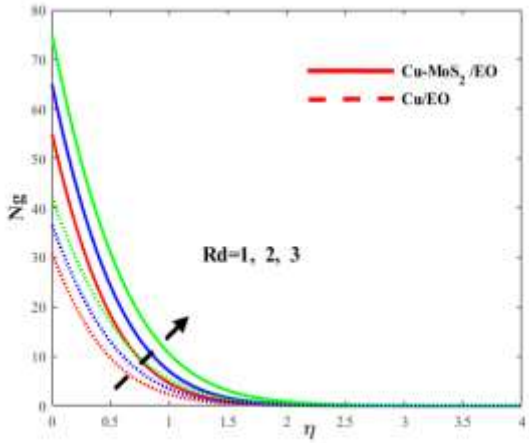

Fig. 28. Change of Rd on N_g.

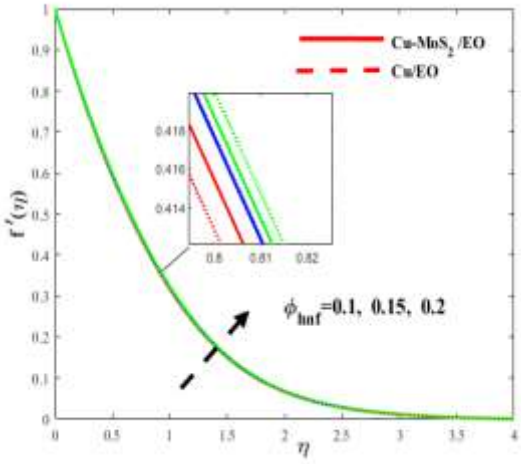

Fig. 29. Change of ϕ_{hnf} on $f'(\eta)$.

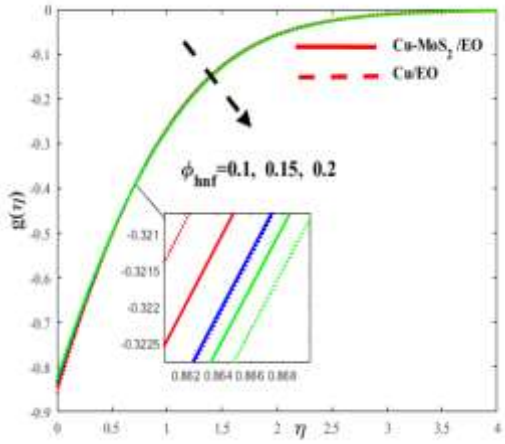

Fig. 30. Change of ϕ_{hnf} on $g(\eta)$.

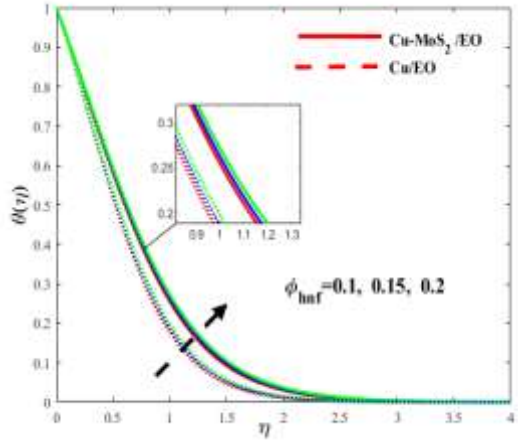

Fig. 31. Change of ϕ_{hnf} on $\theta(\eta)$.

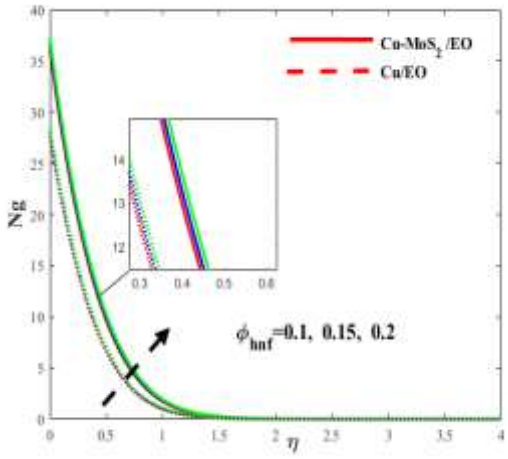

Fig. 32. Change of ϕ_{hnf} on N_g.

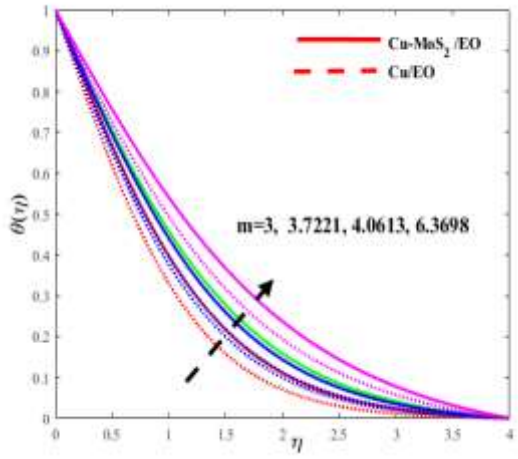

Fig. 33. Change of m on $\theta(\eta)$.

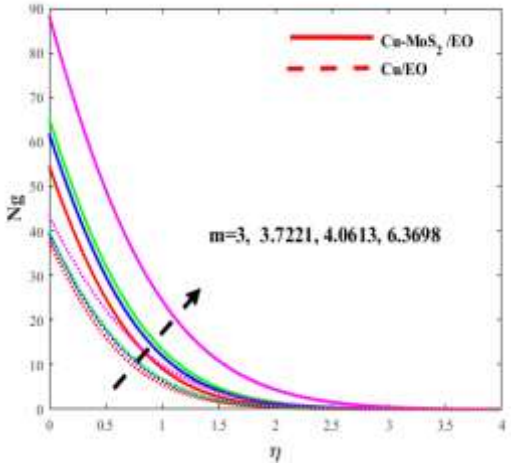

Fig. 34. Effect of m on N_g.

Table 3. Skin friction coefficient against distinct parameters.

ϵ	Pr	Ec	Q	Rd	$Nu_x Re_x^{\frac{-1}{2}}$ Cu-MoS_2/EO	$Nu_x Re_x^{\frac{-1}{2}}$ Cu/EO	Relative % $\frac{Nu_{Cu-MoS_2} - Nu_{Cu}}{Nu_{Cu-MoS_2}}$ %
0.5	7.38	0.1	0.1	0.5	2.5116	2.2088	12.2%
0.7					2.6271	2.3543	10.3%
0.9					2.7211	2.4663	9.3%
0.1					2.8440	2.5577	10.0%
	8				2.6401	2.3184	12.1%
	9				2.8363	2.4858	12.3%
	10				3.0208	2.6433	12.5%
		0.3			2.4341	2.1202	12.9%
		0.5			2.3566	2.0315	13.8%
		0.7			2.2790	1.9428	14.7%
			0.3		2.4126	2.1268	11.8%
			0.5		2.5334	2.2431	11.5%
			0.7		2.5760	2.5133	2.50%
				1	2.9861	2.5968	13.1%
				1.5	3.4857	2.9987	13.4%
				2	3.9255	3.3475	14.7%

Table 4. Heat and mass transport rates with diverse variables.

λ	γ	λ_1	ϵ	Pr	Ec	Q	Rd	m	ϕ_{hnf}	ϕ_2	$f_x Re_x^{\frac{1}{2}}$ Cu-EO	$Cf_x Re_x^{\frac{1}{2}}$ Cu-MoS_2/EO	$Nu_x Re_x^{\frac{-1}{2}}$ Cu-EO	$Nu_x Re_x^{\frac{-1}{2}}$ Cu-MoS_2/EO
0.5	0.5	0.1	0.5	7.38	0.1	0.1	0.5	3	0.18	0.09	0.7289	0.9525	2.2088	2.5116
											0.8872	1.1559	2.2367	2.5646
0.5											0.9957	1.2953	2.2409	2.5725
	1										0.6577	0.8584	2.1712	2.4584
	1.5										0.6403	0.8351	2.1599	2.4429
	2										0.6340	0.8265	2.1556	2.4370
		0.3									0.6023	0.7900	2.2119	2.5100
		0.5									0.2842	0.3930	2.3387	2.6662
		0.6									0.1219	0.1902	2.4043	2.7923
			0.7								0.7289	0.9525	2.3543	2.6271
			0.9								0.7289	0.9525	2.4663	2.7211
			1.1								0.7289	0.9525	2.5577	2.8440
				8							0.7289	0.9525	2.3184	2.6401
				9							0.7289	0.9525	2.4858	2.8363
				10							0.7289	0.9525	2.6433	3.0208
					0.3						0.7289	0.9525	2.1202	2.4341
					0.5						0.7289	0.9525	2.0315	2.3566
					0.7						0.7289	0.9525	1.9428	2.2790
						0.3					0.7289	0.9525	2.1268	2.4126
						0.5					0.7289	0.9525	2.2431	2.5334
						0.7					0.7289	0.9525	2.5133	2.5760
							1				0.7289	0.9525	2.5968	2.9861
							1.5				0.7289	0.9525	2.9987	3.4857
							2				0.7289	0.9525	3.3475	3.9255
								3.7221			0.7289	0.9525	3.5444	4.2633
								4.0613			0.7289	0.9525	3.6328	4.4167
								6.3698			0.7289	0.9525	4.1753	5.3716
									0.09		0.5765	0.7405	2.6577	3.1800
									0.15		0.6692	0.8705	3.1094	3.6694
									0.18		0.7289	0.9525	3.3475	3.9255
										0.0	-	0.7289	-	3.3475
										0.06	-	0.8680	-	3.7333
										0.09	-	0.9525	-	3.9255

5. Concluding remarks

The study presents the novel idea regarding the entropy generation analysis and thermal transport analysis of the SACW by considering hybrid RPNF. Different sundry parameters effect in terms of PTSC and SACW have been deliberated extensively and dispalyed in the tabular and

pictorial procedure. Some salient features of the above mentioned article are summarized underneath

- Heat distrbution phenomenon into SACW improve for the status of diverse parameters ϵ, Rd, Q, m, ϕ_{hnf}, ϕ.
- Hybrid nanofluid Cu-MoS_2/EO is the well exporter of heat transport in comparing to simple nanoliquid Cu/EO for the case of fluid via a PTSC in SACW.
- A magnification in nanoparticles form m enhances heat transfer of fluid past a PTSC.
- Over all system entropy improves for the status of a amplification in λ, Q, Rd, ϕ_{hnf}, ϕ.
- Thermal radiations Rd fall on the surface of PTSC enhances interior energy profiles of SACW.

Nomenclature

Re	Reynold's number	Br	Brinkman's number
T_0	Wall-temperature	T_∞	Ambient-temperature
Ω	temperature variation	λ	penetrability parameter
γ	nanofluid factor	ϵ	variant thermal conductance
Ec	Eckert's number	Cf_x	frictional force
Nu_x	Nusselt's number	Rd	radiative parameter
Pr	Prandtl's number	q_r	heat radiative flux
Q	heat generation parameter	τ_s	reference shear stress
τ	shear stress	α_{hnf}	hybrid-nanofluid thermal diffusion
ρ_{hnf}	hybrid-nanofluid density	k_{hnf}	hybrid thermal conductance
C_p	specific heat at constant pressure	κ^*	absorption coefficient
σ^*	Stefan-Boltzman constant		

Conflict of Interest

The authors pronounce that there is no conflict of interests.

References

[1] X. Wang, Y. He, X. Liu, L. Shi, and J. Zhu. Investigation of photothermal heating enabled by plasmonic nanofluids for direct solar steam generation, *Solar Energy* 157:35-46, 2017.

[2] X. Wang, Y. He, X. Liu, and J. Zhu, Enhanced direct steam generation via a bio-inspired solar heating method using carbon nanotube films, *Powder Technology* 321:276-285, 2017.

[3] X. Wang, Y. He, X. Liu, and J. Zhu, Solar steam generation through bioinspired interface heating of broadband-absorbing plasmonic membranes, *Applied Energy* 195:414-425, 2017.

[4] X. Wang, Y. He, X. Liu, and J. Zhu, Direct vapor generation through localized solar heating via carbon-nanotube nanofluid, *Energy Conversion and Management* 130:176-183, 2016.

[5] A. Noth, R. Siegwart, and W. H. Engel. Design of solar powered airplanes for continuous flight. ETH University, Zurich, Switzerland, 2008.

[6] H. Price, E. Luupfert, D. Kearney, E. Zarza, G. Cohen, and R. Gee, Advances in parabolic trough solar power technology. Journal of Solar Energy Engineering, 109:109-125, 2002.

[7] S.U.S. Choi, Enhancing thermal conductivity of fluids with nanoparticles, *Developments and Application of Non-Newtonian Flows* 66:99-105, 1995.

[8] H. Masuda, A. Ebata, K. Teramae, Alteration of thermal conductivity and viscosity of liquid by dispersing ultra-fine particles by dispersion of Al_2O_3, SiO_2 and TiO_2 ultra-fine particles, *Netsu Bussei* 7:227–233, 1993.

[9] J.A. Eastman, S. Choi, S. Li, W. Yu, L. Thompson, Anomalously increased effective thermal conductivities of ethylene glycol-based nanofluids containing copper nanoparticles, *Applied Physics Letters* 78(6):718-720, 2001.

[10] M.R. Eid, A. Al-Hossainy, M.S. Zoromba, FEM for blood-based SWCNTs flow through a circular cylinder in a porous medium with electromagnetic radiation, *Communications in Theoretical Physics* 71(12):1425, 2019.

[11] S. Lahmar, M. Kezzar, M.R. Eid, M.R. Sari, Heat transfer of squeezing unsteady nanofluid flow under the effects of an inclined magnetic field and variable thermal conductivity, *Physica A* 540:123138, 2020.

[12] M.R. Eid, M.A. Nafe, Thermal conductivity variation and heat generation effects on magneto-hybrid nanofluid flow in a porous medium with slip condition, *Waves in Random and Complex Media* 1-25, 2020. https://doi.org/10.1080/17455030.2020.1810365

[13] S.A. Adio, M. Sharifpur, J.P. Meyer, Factors affecting the pH and electrical conductivity of MgO–ethylene glycol nanofluids, *Bulletin of Materials Science* 38(5):1345-1357, 2015.

[14] S.N. Shoghl, J. Jamali, M.K. Moraveji, Electrical conductivity, viscosity, and density of different nanofluids: An experimental study, *Experimental Thermal and Fluid Science* 74:339-346, 2016.

[15] S.F.M. Nor, N. Azis, J. Jasni, M.Z.A. Ab Kadir, R. Yunus, Z. Yaakub, Investigation on the electrical properties of palm oil and coconut oil based TiO_2 nanofluids, *IEEE Transactions on Dielectrics and Electrical Insulation* 24(6):3432-3442, 2017.

[16] S. Jana, A. Salehi-Khojin, W.-H. Zhong, Enhancement of fluid thermal conductivity by the addition of single and hybrid nano-additives, *Thermochimica Acta* 462(1-2):45-55, 2007.

[17] W. Jamshed, M.R. Eid, N.A.A.M. Nasir, K.S. Nisar, A. Aziz, F. Shahzad, C.A. Saleel, A. Shukla, Thermal examination of renewable solar energy in parabolic trough solar collector utilizing Maxwell nanofluid: A noble case study, *Case Studies in Thermal Engineering* 27:101258, 2021.

[18] A.F. Al-Hossainy, M.R. Eid, Structure, DFT calculations and heat transfer enhancement in $[ZnO/PG+ H_2O]^C$ hybrid nanofluid flow as a potential solar cell coolant application in a double-tube, *Journal of Materials Science: Materials in Electronics* 31(18):15243-15257, 2020.

[19] M.R. Eid, A.F. Al-Hossainy, Combined experimental thin film, DFT-TDDFT computational study, flow and heat transfer in $[PG\text{-}MoS_2/ZrO_2]^C$ hybrid nanofluid, *Waves in Random and Complex Media* 1-26, 2021. https://doi.org/10.1080/17455030.2021.1873455

[20] A.F. Al-Hossainy, M.R. Eid, Combined experimental thin films, TDDFT-DFT theoretical method, and spin effect on $[PEG\text{-}H_2O/ZrO_2+MgO]^h$ hybrid nanofluid flow with higher chemical rate, *Surfaces and Interfaces* 23:100971, 2021.

[21] S.O. Giwa, M. Sharifpur, M.H. Ahmadi, S. Sohel Murshed, J.P. Meyer, Experimental investigation on stability, viscosity, and electrical conductivity of water-based hybrid nanofluid of MWCNT-Fe_2O_3, *Nanomaterials* 11(1):136, 2021.

[22] A. Mojiri, R. Taylor, E. Thomsen, and G. Rosengarten, Spectral beam splitting for efficient conversion of solar energy-a review, *Renewable and Sustainable Energy Reviews* 28:654-663, 2013.

[23] Z. Said and A. Mehmood. Standalone photovoltaic system assessment for major cities of united arab emirates based on simulated results, *Journal of Cleaner Production* 140:2722-2729, 2017.

[24] Z. Said, A. A. Alshehhi, and A. Mehmood. Predictions of uae's renewable energy mix in 2030, *Renewable Energy* 118:779-789, 2018.

[25] E. Bellos, Progress in the design and the applications of linear fresnel re-flectorsea critical review, *Thermal Science and Engineering Progress* 10:112-137, 2019.

[26] M. Ghodbane, E. Bellos, Z. Said, B. Boumeddane, A. Khechekhouche, M. Sheikholeslami, and Z. M. Ali, Energy, financial, and environmental investigation of a direct steam production power plant driven by linear fresnel solar reflectors, *Journal of Solar Energy* 143:021008, 2020.

[27] M. Ghodbane, B. Boumeddane, Z. Said, and E. Bellos, A numerical simulation of a linear Fresnel solar reflector directed to produce steam for the power plant, *Journal of Cleaner Production* 231:494-508, 2019.

[28] G. A. Gonzalez, M. C. Pereira, F. Cuadros, and T. Fartaria. Energy self-sufficiency through hybridization of biogas and photovoltaic solar energy: an application for an Iberian pig slaughterhouse, *Journal of Cleaner Production* 65:318-323, 2014.

[29] E. Kabir, P. Kumar, S. Kumar, A. A. Adelodun, and K. Kim, Solar energy: potential and future prospects, *Renewable and Sustainable Energy Reviews* 82:894-900, 2014.

[30] N. Kannan and D. Vakeesan. Solar energy for future world: A review, *Renewable and Sustainable Energy Reviews* 52:1092-1105, 2016.

[31] C. Luan, Z. Liu, and X. Wang, Divergence and convergence: technology- relatedness evolution in solar energy industry, *Scientometrics* 97:461-475, 2013.

[32] Y. A. Qandile and M. I. Sabry, Guidelines for the treatment of solar energy topics in the unified science curricula of the Gulf Arab states, *Renewable Energy* 14:401-414, 1998.

[33] R. Quitzow, J. Huenteler, and H. Asmussen, Development trajectories in China's wind and solar energy industries: how technology-related differences shape the dynamics of industry localization and catching up, *Journal of Cleaner Production* 158:122-133, 2017.

[34] J. Zhang, Y. Yan, and J. Guan, Scientific relatedness in solar energy: a comparative study between the USA and China, *Scientometrics* 102:1595-1613, 2015.

[35] A. Sciacovelli, V. Verda, E. Sciubba, Entropy generation analysis as a design tool—a review, *Renewable and Sustainable Energy Reviews* 43:1167–1181, 2015.

[36] K. Manjunath, S.C. Kaushik, Second law thermodynamic study of heat exchangers: a review, *Renewable and Sustainable Energy Reviews* 40:348–374, 2014.

[37] M. Torabi, N. Karimi, G.P. Peterson, S. Yee, Challenges and progress on the modelling of entropy generation in porous media: a review, *International Journal of Heat and Mass Transfer* 114:31–46, 2017.

[38] O. Mahian, A. Kianifar, C. Kleinstreuer, A. Al-Nimr Moh'd, I. Pop, A.Z. Sahin, S. Wongwises, A review of entropy generation in nanofluid flow, *International Journal of Heat and Mass Transfer* 65:514–532, 2013.

[39] C. Zhao, S. Zheng, J. Zhang, and Y. Zhang. Exergy and economic analysis of organic rankine cycle hybrid system utilizing biogas and solar energy in rural area of China, *International Journal of Green Energy* 14:123437, 2017.

[40] W. Jamshed, Numerical investigation of MHD impact on Maxwell nanofluid, *International Communications in Heat and Mass Transfer* 120:104973, 2021.

[41] M. G. Reddy, M. V. V. N. L. Sudharani, K. G. Kumar, A. J. Chamkha, and G. Lorenzini, Physical aspects of Darcy-Forchheimer ow and dissipative heat transfer of Reiner-Philippof fluid, *Journal of Thermal Analysis and Calorimetry* 39:11-25, 2019.